JOURNAL OF MATERIALS SCIENCE 33 (1998) 939–953

Fracture in ceramic-reinforced metal matrix composites based on high-speed steel

J. D. BOLTON, A. J. GANT
Department of Mechanical and Manufacturing Engineering, University of Bradford, BD7 1DP UK

A series of metal matrix composites based upon M3/2 high-speed steel was produced by a powder metal sintering route. Hard ceramic titanium carbide or niobium carbide additions and a self-lubricant in the form of manganese sulfide, were added as a basis for achieving improved wear resistance and reduced friction. After sintering, the composites were given a full standard high-speed steel heat treatment and subjected to mechanical tests. All three particulate additions had a deleterious effect on three-point bend strength, particularly in the case of MnS addition, mainly due to the ease of initiating cracks at or near to the particulate additions. Bend strengths were further reduced by the simultaneous addition of both MnS and either TiC or NbC especially when a high volume fraction of approximately 25 vol % MnS was added. Single, low volume fraction ($\leqslant 8\%$) additions, of TiC, NbC, or MnS, had little effect on fracture toughness and K_{IC} values were comparable to those found in the baseline M3/2 steel. Slight improvements in fracture toughness shown to occur in the 7.74% NbC composites were attributed to energy dissipation caused by the effects of crack branching during crack propagation. Composites with the higher volume fraction additions of MnS and ceramic carbide gave poor fracture toughness by forming MnS/carbide clusters which provided an easy path for crack propagation. © *1998 Chapman & Hall*

1. Introduction

This work was undertaken as part of an EU-funded programme and was intended to develop new materials that are capable of operating as diesel engine valve train components under poor or non-lubricated conditions. The objectives of this specific work included an attempt to produce materials for valve seats by using sintered high-speed steels with hard ceramic TiC or NbC carbides and a solid lubricant powder such as MnS incorporated into their structure. The eventual aim of this was to reduce both friction and improve wear resistance but the work undertaken and reported by this paper deals only with an evaluation of the fundamental mechanical properties of a range of sintered M3/2 HSS-based composites and was done as a precursor to any engine or wear performance tests.

2. Experimental procedure

Materials were produced as sintered powder metallurgy metal matrix composites by combining water-atomized AISI M3/2 high-speed steel powder of the composition and particle-size distribution shown, respectively, in Tables I and II, with 5 μm sized titanium carbide (TiC), 4 μm sized niobium carbide (NbC), and or 10 μm manganese sulfide (MnS) powders: 0.25 wt % graphite powder was also added to assist sintering and to make up for carbon losses that occurred during sintering. The range of composite compositions studied is shown in Table III.

Composite powders were mixed by dry blending the constituent powders together in a Y-cone blender for 15 min in batches of 100 g; 15 min was found to be the optimum mixing time, except for the composites which contained NbC, where agglomerated clusters of NbC carbide were still present after dry blending. Wet Y-cone blending under acetone did not improve the distribution of the NbC ceramic carbide particles, but ball milling for 100 h with tungsten carbide balls under acetone and a ball/powder weight ratio of 10 : 1 successfully eliminated agglomeration of NbC carbides. Such lengthy milling times were, however, considered to be impractical, and the ball-milled powders also required further treatment in the form of drying and annealing to eliminate the effects of cold working and to reduce the powder's oxygen content prior to sintering. Granulation of the NbC powder composites with a binder and H-wax before compaction proved to be reasonably successful in eliminating NbC clusters and was the method chosen for producing such composites [1].

Compaction was carried out in a double-acting die at 770 MPa, to produce 15 mm × 15 mm × 4 mm green compacts of approximately 75% theoretical density that were used to evaluate microstructure, sintering, heat treatment and basic mechanical properties. Compaction of specimens used for fracture toughness evaluation was carried out at 650 MPa, using a die operating on the same principle and produced test pieces measuring 52 mm long × 10 mm wide × 3.5 mm thick.

TABLE I Chemical composition of the AISI M3 class 2 high-speed steel powder (wt %)

C	W	Mo	Cr	V	Fe
1.10	6.05	5.80	4.02	2.91	bal.

TABLE II Particle size, analysis of M3/2 high-speed steel powder

Particle size range (μm)	Fraction (%)
0–32	17.4
32–36	4.4
36–45	8.4
45–63	19.2
63–90	27.4
90–125	19.7
>125	3.5

TABLE III Composite (blended) powder mixes

M3 class 2
M3/2 + 5% MnS
M3/2 + 5% TiC
M3/2 + 7.74% NbC
M3/2 + 5% MnS + 5% TiC
M3/2 + 15% MnS + 5% TiC

All specimens were sintered under vacuum (minimum 1×10^{-4} Pa) in a ceramic tube furnace at a temperature capable of producing full density without forming an over-sintered structure with coarse grain-boundary carbides or carbide eutectics. These temperatures were within the range 1240–1260 °C and were highest for the TiC and NbC composites. Each batch of specimens was held for 60 min at their sintering temperature by heating at 10 K min^{-1} and included a 60 min hold period at 1000 °C to facilitate outgassing of the specimens prior to reaching the sintering temperature. After sintering, the specimens were cooled at 5 K min^{-1} to 500 °C, followed by natural furnace cooling to room temperature.

Sintered densities of the sintered specimens were evaluated by a method based on Archimedes principle: the specimens were weighed in air and in water but were coated with a cellulose lacquer to seal surface porosity. An appropriate correction was made to eliminate the mass and volume contribution of the lacquer coating.

Typical full density values achieved by sintering are compared in Table IV with their theoretical density, as calculated from a rule of mixtures: $\rho_t = 1/(X_{hss}/\rho_{hss} + X_c/\rho_c + X_s/\rho_s)$ where ρ_t is the theoretical density, X_{hss} the mass fraction of high-speed steel powder, ρ_{hss} the density of high-speed steel = 8.16 g cm^{-3}, X_c the mass fraction of carbide additive, ρ_c the density of carbide additive (TiC = 4.93 g cm^{-3}, NbC = 7.60 g cm^{-3}), X_s the mass fraction of MnS, and ρ_c the density of MnS = 3.99 g cm^{-3}.

In all cases, the theoretical density calculated by rule of mixtures was slightly different from that produced by sintering, but this simply reflected the fact that the calculated value took no account of any dissolution effects and chemical interactions known to occur between the steel and its particulate addition [2]. Porosity was minimal at the true values of maximum density that were achieved and densities were estimated to be above 99.5% full porosity free value.

TABLE IV Actual and calculated theoretical sintered density of composites studied

Composite	Theoretical maximum density (g cm^{-3})	Actual maximum density (g cm^{-3})
M3/2	8.16	8.16
M3/2 + 5% MnS	7.75	7.76–7.80
M3/2 + 7.74% NbC	8.11	8.18
M3/2 + 5% TiC	7.90	7.88
M3/2 + 7.74% NbC + 5% MnS	7.71	7.76–7.84
M3/2 + 5%TiC + 5% MnS	7.52	7.48
M3/2 + 7.74% NbC + 15% MnS	7.02	7.17–7.22
M3/2 + 5% TiC + 15% MnS	6.86	6.89

2.1. Heat treatment

Some specimens were hardened and tempered before testing by an austenitizing, quenching and tempering process that was carried out in a vacuum heat-treatment furnace equipped with an over-pressure gas-quench facility. Austenitization was performed under vacuum (minimum 6×10^{-3} mbar), with two 10 min preheats at 850 and 1050 °C to minimize the risk of distortion and promote the solution of carbides, followed by holding for 7 min at a final austenitizing temperature which was chosen as that thought capable of giving the maximum as-quenched hardness. This temperature lay within the range 1150–1220 °C and tended to be higher for composites that contained either TiC or NbC carbides. Quenching to room temperature under high-pressure flowing nitrogen was immediately followed by a double tempering treatment carried out in the same furnace, at temperatures in the range 450–600 °C, with each temper lasting for 1 h.

2.2. Bend strength

Transverse rupture strength was evaluated in three-point loading, with the transverse rupture strength (TRS value) being determined from simple elastic bending theory equations; plastic deformation was justifiably ignored on the basis that the high-speed steel alloys exhibited brittle behaviour.

Bend test specimens, with dimensions 15 mm × 3.5 mm × 3 mm, were machined, ground with silicon carbide grit papers, and finally diamond polished down to a 1 μm finish on the tensile face. Test specimens were supported by cemented carbide rollers of diameter 4 mm and span 12 mm and tested at a cross

head speed of 0.1 mm min^{-1}

$$\sigma_f = \frac{3PL}{2BD^2} \quad (1)$$

where P is the load, L the span, B the specimen width, and D the specimen depth.

2.3. Fracture toughness

Fracture toughness testing was carried out according to the guidelines and parameters laid down in British Standard BS 5447 [3], which specifies the required specimen dimensions, yield strength and specimen ductility to obtain plane strain conditions. Fatigue cracking could not be used to obtain a pre-crack in the brittle high-speed steel materials under investigation, but use was made of an alternative method, usually accredited to Eriksson [4]. The method involved the application of compressive force, of around 1.0 GPa, on faces either side of a 45° chevron notch cut into one edge of the test piece, followed by impact loading applied to a cemented carbide chisel placed in the mouth of the chevron notch, by allowing a 70 g weight to fall on to the chisel from a height of between 60 and 120 cm. Impact induces the formation of a sharp-tipped crack at the root of the notch but its propagation and final length were arrested by the compressive force applied across the crack flanks.

Specimens for fracture toughness testing were made from heat-treated blanks, approximately 52 mm × 12 mm × 3.5 mm, that were further sliced into four with a diamond wafering blade and then ground to the final dimensions of 25 mm long × 6.0 mm wide × 2.8 mm thick. Each pre-cracked specimen was inspected under a binocular microscope to check the pre-crack length, a, to specimen width, W, and that the a/W ratio lay within the limits $0.35 < a/W < 0.6$. Specimens which satisfied the pre-crack length criterion were also etched in 5% nital for 5 min before testing, to aid measurement of crack length by staining of the pre-crack surfaces. Testing was performed in three-point bending on a tensile testing machine at a crosshead speed of 10 mm min^{-1}, with a span between outer rollers of 24 mm. Fracture toughness was calculated from the formula

$$K_{Ic} = 3\,PL\,Y/(BW)^{3/2} \quad (2)$$

where P is the load, B the breadth (3 mm) and W the depth of the sample (6 mm). $2L$ is the effective span (i.e. across the outer rollers): 24 mm. Y, the calibration function for three-point bending [5, 6], is given by

$$Y = 1.93\,(a/W)^{0.5} - 3.07\,(a/W)^{1.5} + 14.53\,(a/W)^{2.5} - 25.11\,(a/W)^{3.5} + 25.8\,(a/W)^{4.5} \quad (3)$$

The crack front in most samples was of a "thumbnail" shape and was measured at five equispaced intervals across its width to determine a mean value for a/W.

2.4. Evaluation of Young's modulus

Young's modulus values were determined for the various composites by an ultrasonic method that measured the speed of ultrasonic waves through the test sample and was evaluated directly from the equation

$$\rho\,\mu_L^2 = E(1-\nu)/(1+\nu)(1-2\nu) \quad (4)$$

where ρ is the density, ν the poisson's ratio, E Young's modulus and u_L the shear wave velocity.

The wave velocity can be determined in a number of ways [7], the simplest being the time of flight of the first pulse, or the time delay between successive face-to-face reflections. Good agreement with static measurements of elastic modulus occurs when the wavelength is long compared to the dimensions of any micro-structural features, as was the case for the high-speed steel composites under investigation.

3. Results

3.1. Mechanical properties of as-sintered materials

3.1.1. Hardness

Hardness results for both bulk Vickers macro-hardness, H_v, and the micro-hardness, H_m, of the high-speed steel matrix of the fully dense sintered composites have been previously reported elsewhere [8], and are also summarized in Table V.

All of the composites which contained MnS additions had low bulk hardness due to the collapse of MnS particles beneath the indentor. Appreciable softening of the matrix also occurred in some composites produced with an impure grade of MnS which was largely caused by high oxygen contents of the MnS powder and the the subsequent decarburization of the steel matrix. Later composites produced by using a purer grade of MnS did not experience such a marked decarburization of the steel matrix.

Optimum hardening and tempering temperatures varied between the different composites [8]: baseline M3/2 HSS or M3/2 + TiC composites were best quenched from 1180 °C and tempered at 550 °C, whereas the M3/2 + NbC composites were best quenched from 1180 °C and tempered at 525 °C. The highest hardness values achieved by secondary hardening occurred in the M3/2 + NbC composites, i.e. 900 H_v (1000 H_m matrix), compared with 860 (880 H_m matrix)

TABLE V Bulk macro-hardness and matrix micro-hardness of materials in the as-sintered condition

Material	Macrohardness, H_v30	Microhardness H_m matriz
Baseline M3/2	563 ± 9	612 ± 48
M3/2 + 5% TiC	612 ± 5	602 ± 42
M3/2 + 7.74% NbC	622 ± 4	637 ± 61
M3/2 + 5% MnS	499 ± 9	533 ± 43
M3/2 + 5% TiC + 5% MnS	521 ± 10	606 ± 51
M3/2 + 7.74% NbC + 5% MnS	574 ± 9	667 ± 47
M3/2 + 5% TiC + 15% MnS	404 ± 6	615 ± 43
M3/2 + 7.74% NbC + 15% MnS	437 ± 8	630 ± 37

and 875 H_v (850 H_m matrix) for the baseline M3/2 and M3/2 + TiC composites, respectively. The matrix micro-hardness of the M3/2 + NbC composite was also found to be higher than that of the baseline material, whereas the matrix of the M3/2 + TiC composite was actually slightly softer than that of the baseline M3/2 matrix. MnS additions caused a significant drop in the peak hardness produced by secondary hardening, i.e. 670 H_v and 840 H_m matrix hardness.

3.1.2. Bend strength: as-sintered

Table VI shows the effect of particulate additions (singly and as double additions) on transverse rupture strength of composites sintered to full density with an optimum microstructure. All additions made to the M3/2 baseline steel reduced bend strength and additions of MnS had a particularly deleterious effect on strength. Single additions of either TiC or NbC also reduced bend strength but NbC additions had a less marked effect than TiC. Ball milling of composites containing NbC also produced a significant improvement in bend strength compared with the blended composites of the same composition.

Double additions of mono-carbide and MnS produced a significant drop in bend strength, particularly with the 15 wt % addition of MnS, but the composite that contained NbC in place of TiC again gave higher strength values.

3.1.3. Bend strength: Heat treated

Transverse rupture strengths of the various composites in their optimum heat-treated conditions are shown in Table VII. Bend strength values were generally higher after heat treatment than with the as-sintered composites, but the results revealed a similar pattern of diversity in bend strength to those reported for the as-sintered composites. Additions of MnS had a most deleterious effect on transverse rupture strength and the reduction in TRS caused by TiC addition was more pronounced than the effect of adding NbC. Ball milling of composites containing NbC again produced a significant improvement in bend strength compared with blended composites of the same composition.

Double additions of mono-carbide and MnS produced a larger drop in bend strength especially with the larger 15 wt % addition.

TABLE VI Transverse rupture strengths of materials in the as-sintered condition

Material	Mean TRS (GPa)	Range (GPa)
Baseline M3/2	2.18	2.09–2.24
M3/2 + 5% TiC	1.82	1.79–1.88
M3/2 + 7.74% NbC	1.87	1.81–1.89
M3/2 + 7.74% NbC[a]	2.30	2.24–2.32
M3/2 + 5% MnS	1.11	1.03–1.21
M3/2 + 5% TiC + 5% MnS	1.13	0.98–1.25
M3/2 + 7.74% NbC + 5% MnS	1.14	1.13–1.35
M3/2 + 7.74% NbC + 5% MnS[a]	1.24	1.22–1.30
M3/2 + 5% TiC + 15% MnS	0.593	0.59–0.60
M3/2 + 7.74% NbC + 15% MnS	1.16	1.09–1.22

[a]Ball milled materials.

TABLE VII Transverse rupture strengths of materials, in the quenched and tempered condition

Material	Mean TRS (GPa)	Range (GPa)
Baseline M3/2	2.68	2.23–3.18
M3/2 + 5% TiC	1.83	1.54–2.25
M3/2 + 7.74% NbC	1.91	1.63–2.25
M3/2 + 7.74% NbC[a]	2.43	2.24–2.57
M3/2 + 5% MnS	1.71	1.04–2.38
M3/2 + 5% TiC + 5% MnS	1.26	0.95–1.59
M3/2 + 7.74% NbC + 5% MnS	1.14	0.97–1.40
M3/2 + 7.74% NbC + 5% MnS[a]	1.47	1.38–1.54
M3/2 + 5% TiC + 15% MnS	0.72	0.66–0.81
M3/2 + 7.74% NbC + 15% MnS	0.75	0.69–0.86

[a]Ball milled materials.

3.1.4. Weibull analysis of bend test data

Weibull statistics [9, 10], were used to analyse the bend strength data for the high-speed steel composites on the basis that such materials are macroscopically brittle materials and that fracture can be initiated by numerous types of flaw or defect that can cause stress concentration. Typical Weibull plots representative of TRS test data obtained with heat-treated composites are shown in Fig. 1a–d. The steeper slope shown by the line which fitted the majority of the data shown in Fig. 1a–d was used to signify the Weibull modulus, m, shown in Table VIII, and represents a measure of the scatter and the reliability of the bend strength data of each material under stress.

Large values of m denote a more reliable material and indicate that only small changes in the shape and size of failure-initiating defects have resulted from the introduction of either particulate addition or from variations in the sintering/heat-treatment conditions. Shallower line gradients and smaller Weibull moduli towards the lower stress end of the bend strength data, shown in Fig. 1a–d, possibly indicated that failure was initiated by different types of defect and that not all the bend strength values obtained could be attributed to the initiation of failure by one single type of defect.

The Weibull modulus for the baseline material obtained was consistent with that found by Beiss *et al.* [11], for M2 high-speed steel [12], but no previous results appear to exist for M3/2 HSS. Small volume fractions of second-phase MnS or ceramic carbide additions, lowered the Weibull modulus, thus indicating that the strength of these composites was less

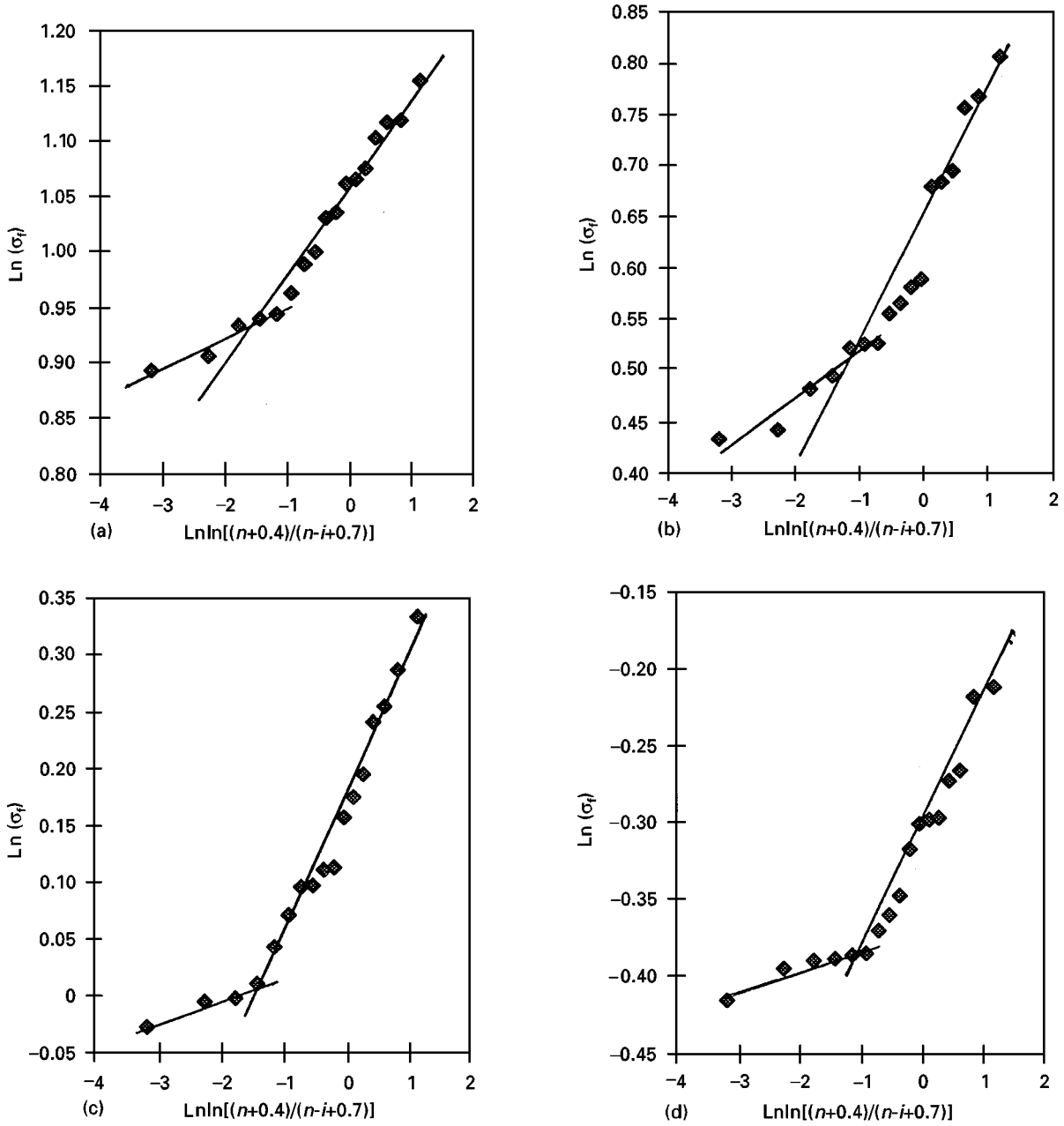

Figure 1 Weibull plot of bend strength data. (a) M3/2 baseline high-speed data. (b) M3/2 HSS + 5% TiC. (c) M3/2 HSS + 5% MnS + 7.74% NbC. (d) M3/2 HSS + 15% MnS + 5% TiC.

TABLE VIII Weibull moduli for heat-treated M3/2 baseline material and composites

Material	Sintering temp (°C)	Sample number, *n*	Weibull modulus, *m*	Characteristic stress σ_o (GPa)
M3/2	1240	17	14.78	2.872
M3/2 + 5% TiC	1255	17	8.33	1.900
M3/2 + 7.74% NbC	1250	15	13.0	2.014
M3/2 + 5% MnS	1250	15	[a]	1.840
M3/2 + 5% TiC + 5% MnS	1275	17	8.75	1.363
M3/2 + 7.74% NbC + 5% MnS	1270	17	11.1	1.206
M3/2 + 5% TiC + 15% MnS	1285	17	11.3	0.735
M3/2 + 7.74 NbC + 15% MnS	1280	25	[a]	0.758

[a]Weibull moduli not calculated due to excessive scatter of data

predictable. Differences in effect between the various particulate additions also occurred, namely that composites containing NbC (whether or not MnS is additionally present) gave higher Weibull moduli than the equivalent composites that contained TiC. The Weibull moduli of the composite materials were still within the range found by previous workers for high-speed steels [11–13].

3.1.5. Plane strain fracture toughness, K_{IC}

Fracture toughness values were determined from a series of quenched and tempered composites that were hardened to different hardness levels by tempering within a tempering temperature range of 450–600 °C. Relationships between these fracture toughness values and either the bulk macro-hardness or matrix micro-hardness of the composites were complex, see Fig. 2a and b. An inverse linear relationship, with a reasonably good fit, existed between fracture toughness and micro-hardness for the baseline M3/2 material and the composites which contained single additions of ceramic carbide; micro-hardness data gave the best fit between these data, see Fig. 2b. Fracture toughness was relatively insensitive to changes in micro-hardness in the composite materials that contained a mixture of carbide plus MnS, and almost no correlation existed between fracture toughness and bulk macro-hardness for any of the composites tested, especially with those which contained ceramic carbide and a high volume fraction of MnS.

The significant scatter in data clearly meant that little meaning could be attached to any relationship between fracture toughness and bulk hardness, especially in the case of composites which contained both the 5 or 15 wt %, MnS addition, although fracture toughness values in composites which contained MnS were consistently lower than those given by the baseline material at the same matrix micro-hardness.

Measured K_{IC} values for the M3/2 baseline material were in good agreement with published data [14], and linear regression analyses [10], gave a linear relationship with reasonably good correlation between K_{IC} fracture toughness and the matrix micro-hardness of the M3/2 baseline material: namely $K_{IC} = 59.59 - 0.043\ H_m$ (correlation coefficient 0.826).

This relationship was used to calculate K_{IC} values for the various composite materials equivalent to that of the M3/2 baseline high-speed steel at an equal value of matrix micro-hardness and was intended to represent the fracture toughness that the composite might be expected to achieve if toughness was only dependent on the hardness of the high-speed steel matrix, see Table IX.

Table IX shows that the value of fracture toughness for the 5% TiC material corresponded exactly to that of the expected M3/2 baseline high-speed steel of similar matrix hardness. Fracture toughness in the 7.74% NbC and 5% MnS composites were, respectively, slightly above and slightly below those of the baseline. The fact that K_{IC} values obtained in composites that contained ceramic carbides combined with either 5% or 15% MnS additions were far lower than those calculated from the regression analysis, see Table IX, was thought to be a real and acceptable effect, despite the fact that the fracture toughness data for these materials was extremely scattered.

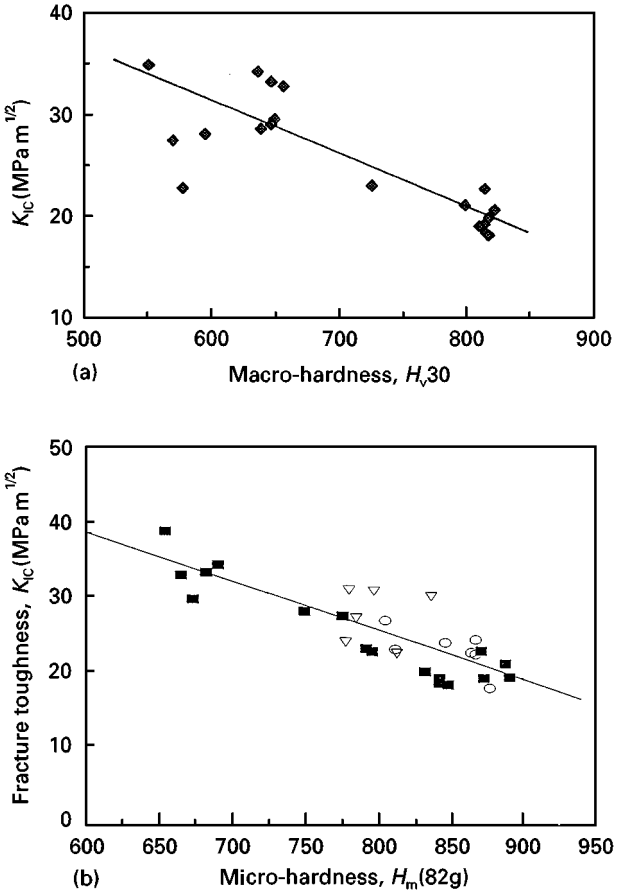

Figure 2 (a) Fracture toughness K_{IC}, versus bulk macro-hardness in quenched and tempered M3/2 HSS. (b) Fracture toughness, K_{IC}, versus micro-hardness in quenched and tempered M3/2 HSS and in composites containing single, low volume fraction, carbide additions. (■) Baseline M3/2 HSS, (○) M3/2 HSS + 5% TiC, (▽) M3/2 HSS + 7.74 % NbC.

3.1.6. Critical strain energy release rate

K_{IC} values are not a true measure of toughness and cannot be used to compare toughness between materials with different Young's moduli, e.g. as in the case of comparative studies of toughness in cemented carbides and high-speed steels. The lower Young's modulus of high-speed steels causes them to have significantly better toughness than cemented carbides, despite having similar K_{IC} values to cemented carbides. True toughness is more properly measured by G_{IC}, the critical strain energy release rate at fracture, but this requires knowledge of the effects of the

TABLE IX Comparison of fracture toughness values in composites with expected baseline K_{IC} values at the same matrix micro-hardness (from regression analysis)

Material	Mean micro-hardness, H_m	Measured K_{IC} (MPa m$^{1/2}$)	Calculated K_{IC} for M3/2 HSS (MPa m$^{1/2}$)
M3/2 + 5% TiC	847	23.3	23.2
M3/2 + 7.74% NbC	799	27.83	25.2
M3/2 + 5% MnS	714	24.62	28.9
M3/2 + 5% TiC + 5% MnS	652	21.8	31.6
M3/2 + 7.74% NbC + 5% MnS	752	23.0	27.3
M3/2 + 5% TiC + 15% MnS	678	13.1	30.4
M3/2 + 7.74% NbC + 15% MnS	717	14.3	28.8

TABLE X Young's modulus of M3/2 HSS composites determined by ultrasound

Material	Measured values: Young's modulus (GPa)
M3/2 Baseline alloy	225
M3/2 + 5% TiC	223
M3/2 + 7.74% NbC	223
M3/2 + 5% MnS	184
M3/2 + 5% TiC + 5% MnS	190
M3/2 + 7.74% NbC + 5% MnS	193
M3/2 + 5% TiC + 15% MnS	174
M3/2 + 7.74% NbC + 15% MnS	178

particulate additions on the Young's modulus of the high-speed steel composite. Values of Young's modulus were measured on fully dense heat-treated specimens by ultrasonic methods, using Equation 1 and a typical value of Poisson's ratio for steel equal to 0.3. The results shown in Table X, agreed well with the available published values for M3/2 baseline high-speed steel [15], but published data were not available for any of the composites. The results indicated that small single (< 8 vol %) additions of mono-carbide had no significant effect on Young's modulus, but that Young's modulus was markedly reduced by the addition of MnS.

Calculated values of Young's modulus, based on published values for the Young's modulus of 104, 352 and 430 GPa for each respective MnS, NbC and TiC particulate component [16,17], were determined via rule of mixtures relationships suitable for both an upper bound (iso-strain) and lower bound (iso-stress) condition in fibre composites [18]. All of the calculated Young's modulus values, including those calculated at a lower bound condition, were too high and gave nothing like reasonable agreement with measured values. The tendency for calculated Young's moduli to be too high was not unexpected, firstly because of phase interactions known to exist between the high-speed steel and the ceramic carbide which led to reductions in the volume fraction and to changes in the composition of the ceramic carbide particles, and secondly because of debonding at the MnS/steel interface that was produced by interfacial stresses introduced by differences in thermal contraction during cooling from the sintering temperature: the coefficient of thermal expansion coefficient of MnS is greater than steel [16].

Critical strain energy release rates, G_{IC}, were calculated using the relationship [17]

$$G_{IC} = (K_{IC}^2/E)\,(1 - \nu^2) \quad (5)$$

where ν is Poisson's ratio, E the measured Young's modulus, and K_{IC} the fracture toughness, but only in the case of the composites which contained MnS particles, principally because their Young's moduli differed significantly from that of the M3/2 baseline material. Similar comparisons to those used to determine K_{IC} as a function of matrix micro-hardness served to emphasize the findings that toughness was lower than predicted in the composites that contained MnS, especially for the double addition composites which contained the higher 15% MnS addition, see Table XI.

TABLE XI G_{IC} toughness found in composites which contained MnS compared with G_{IC} toughness calculated as a predicted value for the M3/2 baseline material at the same matrix micro-hardness

Material	Matrix micro-hardness, H_m	Measured G_{IC} (kJ m^{-2})	Calculated G_{IC} (kJ m^{-2})
M3/2 + 5% MnS	714	2.99	3.38
M3/2 + 5% TiC + 5% MnS	652	2.28	4.04
M3/2 + 7.74% NbC + 5% MnS	752	2.49	3.01
M3/2 + 5% TiC + 15% MnS	678	0.90	3.74
M3/2 + 7.74% NbC + 5% MnS	717	1.05	–

3.2. Fractographic examination

3.2.1. Crack propagation

Fracture surfaces of the broken three-point bend test specimens were examined by scanning electron microscopy to determine possible failure initiation sites and the principal fracture propagation modes.

Failure initiation sites could not be easily identified in most of the bend specimens and fracture initiation could not be definitely linked to any isolated single phase within the microstructure. Second-phase additions, such as TiC, NbC carbides, or MnS clusters, however, were often present at sites where failure initiation was thought to have occurred and were usually located at or near to, the surface of the tensile face of the specimens, see Fig. 3.

Crack propagation through the baseline M3/2 material mainly consisted of transgranular cleavage through the matrix but a few isolated areas of ductile failure, due to localized plasticity, also occurred, see Fig. 4. Cleavage failures were evident across numerous M_6C carbides that lay on the fracture surface, but crack propagation near to any MC carbides occurred by debonding at the carbide/matrix interface, rather than by cleavage across the carbide, see Fig. 4.

Crack propagation through the matrix of the M3/2 + TiC composite was similar to that found in the baseline alloy and also showed clear evidence of cleavage fracture across carbide clusters that contained a mixture of TiC and MC carbides, see Fig. 5. These carbide clusters were formed by an interaction between the TiC particles and the steel matrix during sintering, which led to the formation of MC carbides at the steel/TiC interface and the replacement of M_6C by MC carbides within the high-speed steel matrix [2].

Niobium carbides were also modified in composition by diffusion of vanadium from the steel into the NbC particles during sintering [2]. Clusters of these carbides with multi-faceted cleavage fractures were seen on the fracture surface, see Fig. 6.

Examination of the fracture surfaces of the MnS single addition composite showed that significant

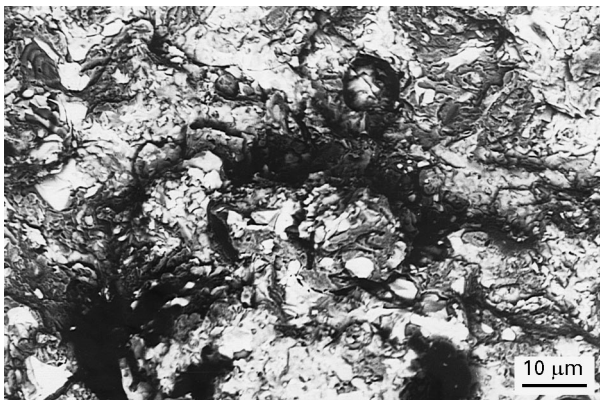

Figure 3 Possible fracture initiation site at the tensile face of a broken M3/2 HSS + 7.74% NbC bend test specimen. BSE image.

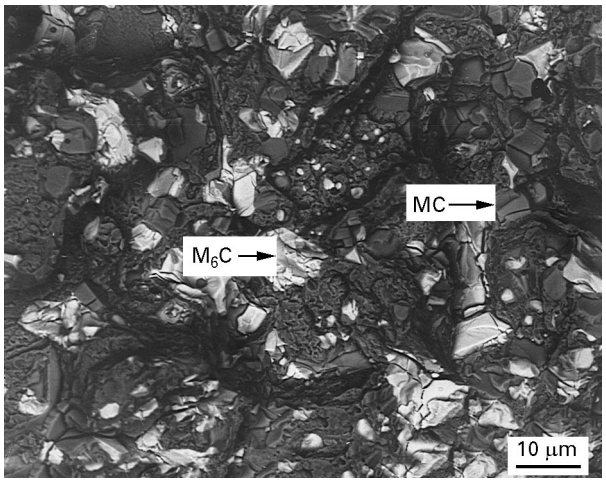

Figure 4 Fracture surface of M3/2 HSS baseline alloy. Note areas of ductile fracture and the numerous M_6C carbides on the fracture surface. BSE image.

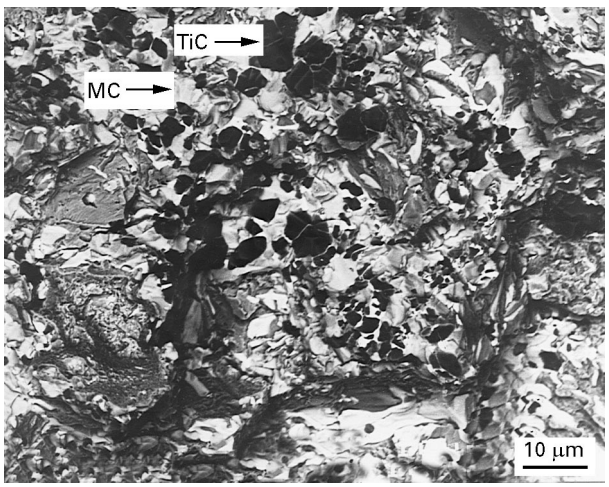

Figure 5 Fracture surface of M3/2 HSS + 5% TiC composite. Note cleavage fracture within TiC/MC clusters. BSE image.

levels of debonding between the MnS particle and its high-speed steel matrix had occurred and this gave rise to the formation of pore-like craters on the fracture surface. Occasional evidence of cleavage across MnS particles was also seen, see Fig. 7.

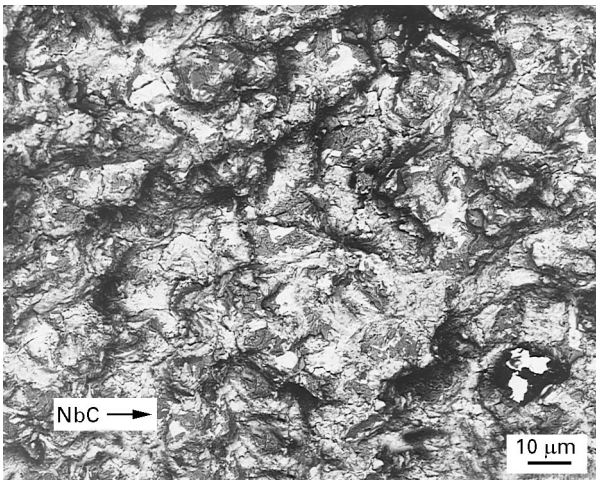

Figure 6 Fracture surface of M3/2 + 7.74% NbC composite. Note NbC clusters of the fracture surface.

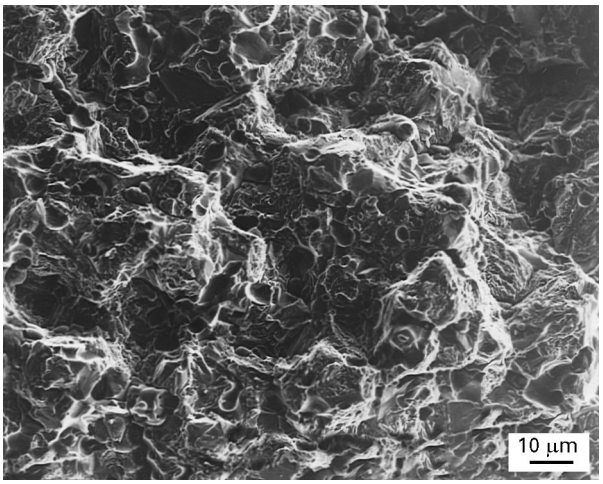

Figure 7 Fracture surface of M3/2 + 5% MnS composite. Note pore-like craters produced by debonding around MnS particles. BSE image.

Debonding between the MnS particle and its high-speed steel matrix also occurred in composites which contained the double addition of MnS plus ceramic carbide but significant number of MnS particles also remained held *in situ* on the fracture surface, especially within the M3/2 + MnS + TiC composites, see Fig. 8. This was perhaps indicative of better bonding between the steel and the MnS particles, when TiC carbides were also present: previous work has shown that little bonding by chemical interaction occurred between particles of MnS and the high-speed steel matrix during sintering, but that a titanium-rich surface layer could form at the steel/MnS particle interface when TiC was also present. This layer was thought to form by chemical interaction between the MnS and TiC particles and was eventually shown to develop into the formation of $Ti_4C_2S_2$ phases, if the sintering temperature was high enough [2, 19].

The main crack did not deviate far from a path perpendicular to the applied stress and made no attempt to follow a preferred path through any of the second-phase additions, except in the case of the composites with high 15% additions of MnS. In these composites the crack travelled preferentially through

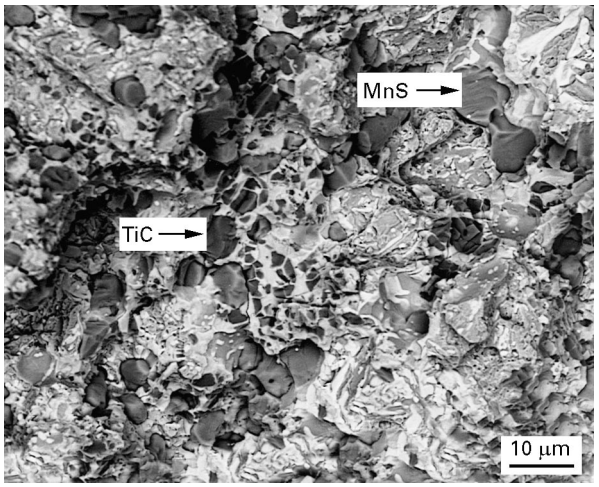

Figure 8 Fracture surface of M3/2 + 5% MnS + 5% TiC composite. Note cleavage across TiC/MC clusters, debonding around MnS particles and the retention of some MnS particles on the fracture surface. BSE image.

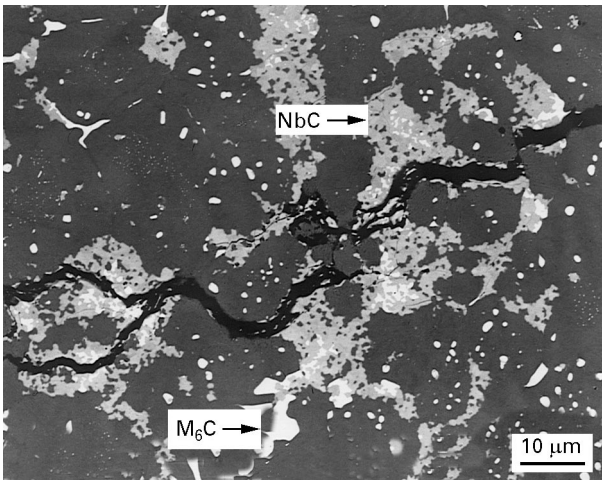

Figure 10 Branching cracks formed within the NbC clusters and ahead of the main pre-crack of a fracture toughness test piece, M3/2 + 7.74% NbC composite. BSE image.

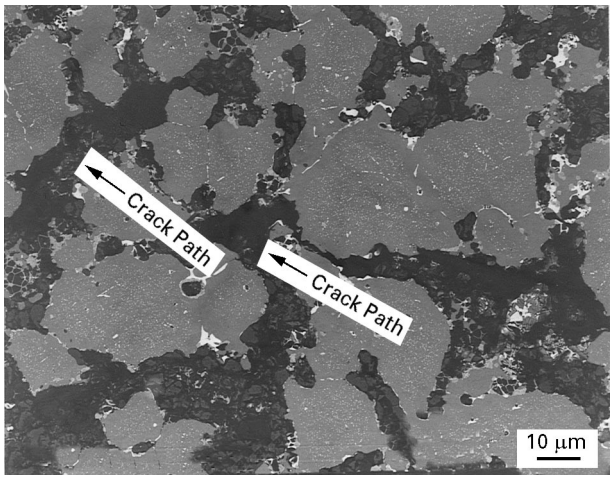

Figure 9 Transverse section through the pre-crack path of an M3/2 + 5% TiC + 15% MnS fracture toughness testpiece. Crack path, shown by arrows, follows the MnS/carbide network. BSE image.

a network of MnS/TiC or MnS/NbC clusters, and this was shown particularly well by examination of the paths taken by the pre-cracks produced for fracture toughness testing, see Fig. 9.

Secondary cracking, both as cracks branching off from the main crack and as subsidiary crack systems formed ahead of the main crack, were also observed on the pre-cracked fracture toughness test pieces. Significant crack branching and cracking ahead of the main crack tip were seen within the M3/2 + 7.74% NbC composite and was often formed in association with NbC clusters that were isolated from the main crack and at some distance ahead of the main crack tip, with a considerable extent of crack branching within NbC clusters themselves, see Fig. 10. No unambiguous evidence of cracking ahead of the main pre-crack or crack branching was found in composites that contained ceramic particle clusters such as MnS/TiC or TiC/MC; any cracks that might possibly have been present were extremely difficult to distinguish within the dark coloured background of the TiC/MnS clusters and were easily masked by other features, such as inter-particle boundaries.

3.2.2. Crack nucleation

Microcracks were seen on the polished tensile faces of heat-treated three-point bend test specimens after testing, and at some distance away, >100 μm, from the point where complete fracture occurred. These cracks were found to occur in both the high-speed steel matrix and inside either of TiC, NbC ceramic carbides, or within the MnS/carbide clusters seen in the composite materials.

Typical values of the fibre stress present at a microcrack found on the tensile face were calculated by determining their location relative to the position of the outer rollers and the point of maximum bending applied during the three-point bend test. These are shown in Table XII, alongside an identification of the feature responsible for creating the microcrack. Subcritical microcracks formed in the M3/2 baseline material at stress levels of around 85% of the final fracture strength and were predominantly found in the M_6C carbides, although they usually also traversed into the surrounding steel matrix and cracks were also found within the MC carbides. Microcracks found in the 5% TiC or 7.74% NbC composite material were either mainly nucleated within TiC/MC carbide clusters, at about 95% of the final fracture strength, or within NbC clusters and in adjacent matrix areas at a slightly lower proportion of the final fracture strength. In the case of the composites which contained either TiC or MnS, cracks were almost always only found inside the TiC or MnS second phases and rarely traversed into the HSS matrix. Cracks found within the NbC-based composite were associated with clusters of NbC carbide but also often traversed into any intervening matrix regions near to the NbC cluster.

Crack initiation was far easier in composites that contained MnS and mainly took place by debonding at the MnS/matrix interface. The stress levels required

TABLE XII Stress to generate microcracking at various microstructural features present on the polished tensile face of broken bend test samples

Material	Location of microcrack	Stress to nucleate microcrack (GPa)	Ratio of stress to form microcrack/bend strength
Baseline M3/2 HSS	M_6C carbide particle	2.40	0.85
	Matrix and M_6C/MC carbide	2.23	0.78
M3/2 + 5%TiC	TiC particle	1.53	0.94
	TiC/MC cluster	1.74	0.955
	MC carbide	1.47	0.95
	Pore	1.76	0.80
M/32 + 7.74% NbC	NbC carbide cluster	1.59	0.87
	Matrix and NbC	1.70	0.93
M3/2 + 5% MnS	MnS/matrix interface	1.19	0.58
M3/2 + 5% MnS + 5% TiC	Matrix	1.44	0.82
	Matrix/TiC/MnS cluster	1.37	0.98
	TiC	0.94	0.71
M3/2 + 7.74% NbC + 5% MnS	NbC/MnS interface	0.85	0.85
	MC/matrix interface	0.83	0.79
	Traverse of MnS/Matrix/MC	0.96	0.89

to nucleate cracks at MnS particles were lower than in any other composite, both in terms of the actual stress and as a fraction of total bend strength, although the stress needed to initiate microcracking in the MnS phase was raised slightly when TiC was also present, see Table XII. This was possibly due to better bonding formed by the reaction which produced a titanium rich interface at the matrix/MnS/TiC interface [19].

Further analysis of crack initiation was performed by examination of the polished tensile face in bend test samples, for evidence of cracks after stopping the load at set intervals below the expected failure stress: the polished face was also sputter coated with iron oxide to enhance colour contrast between the carbide and particulate additions [20].

Sites at which microcracks were first seen in the composites were invariably associated with the TiC, NbC, and/or MnS particles or with M_6C and MC primary carbides of the M3/2 baseline material. Cracks were often seen to grow from their initial carbide or MnS particle into the surrounding steel matrix and surprisingly low stress levels, of only approximately 60% of the final bend strength, were required to develop the first observable cracks in either the ceramic carbide or the MnS particles. Cracks were not seen in the primary M_6C or MC carbides of the M3/2 baseline steel until stresses nearer to 80% of final bend strength were reached.

4. Discussion

4.1. Mechanical properties

4.1.1. Hardness

The effects of adding ceramic carbides and MnS on the hardness of M3/2 high-speed steel have already been discussed elsewhere [8], but their effects on hardness can be briefly summarized as follows.

Hard ceramic carbide additions, such as TiC and NbC, gave rise to only a slight increase in the overall bulk macro-hardness, principally because only small volume fractions (8 vol %) of hard carbide phase were present, so that the overall bulk macro-hardness was dictated mainly by the hardness of the high-speed steel matrix. Relatively small volume fractions of MnS addition apparently reduced overall bulk hardness, but this was partially an artificial effect caused by the collapse of MnS particles and of any surrounding but poorly bonded matrix beneath the hardness indentor. Effectively, the MnS particles behaved in a similar manner to that found when pores collapse beneath the indentor after the hardness testing of porous materials. More significant effects on hardness were noted when the micro-hardness of the matrix instead of the overall bulk hardness was measured. Micro-hardness reflected the changes in hardness developed within the high-speed steel caused by its chemical interaction with the particulate addition and helped to highlight any accompanying changes in composition, microstructure, and heat-treatment response.

Manganese sulfide remained more or less inert with respect to the steel and had little effect on matrix hardness or heat-treatment response, except when allowed to introduce oxygen as an impurity and to cause decarburization of the steel matrix.

Titanium carbide additions also caused only minor changes in hardness and actually produced some slight softening of the high-speed steel matrix by promotion of the replacement of M_6C by MC carbides within the steel matrix. The formation of MC carbide effectively tied up more of the available carbon in a combined state and provided a less soluble form of primary carbide, so that the less highly alloyed martensite formed by quenching was less capable of producing secondary hardening after tempering. At the same time, little solution of any titanium into the steel

matrix took place so that dissolved titanium did not take part in or modify the carbide precipitation reactions responsible for the hardening that took place by secondary hardening after tempering.

Niobium carbide additions were effective in raising the peak hardness of the matrix after quenching and tempering and reduced the tempering temperature required to achieve the maximum secondary-hardening effect. No explanation for this is yet available but there was evidence that niobium had some slight solubility in the austenite formed prior to quenching which led to the speculation that the combination of vanadium plus niobium carbides dissolved into the as-quenched martensite may have produced changes in the composition, morphology and stability of the carbide precipitates responsible for the peak secondary-hardening effects [2].

4.1.2. Fracture toughness

Relatively little work has previously been done to measure the plane strain fracture toughness of M3/2 high-speed steel compared with other grades of high-speed steel but the values for K_{IC} obtained with the baseline M3/2 material were comparable with those of other authors [21]. The mean value of K_{IC} was approximately 18 MPa $m^{1/2}$, when heat treated by quenching and tempering to produce the highest obtainable hardness, but higher values than this and nearer to 30 MPa $m^{1/2}$ were obtained in the baseline M3/2 high-speed steel at lower hardness, such as those seen in the as-sintered state. Reasonable correlation existed between hardness, and fracture toughness in the baseline material both in terms of overall bulk hardness, which included the contribution made by primary carbides, and also with the micro-hardness of the steel matrix which only represented the hardness of any tempered martensite. The inverse type relationship shown by these results was of the expected form and confirmed that K_{IC}, fracture toughness, was reduced by any restriction in the size of the plastic zone formed at the crack tip and by any inherent difficulty of forming a plastic zone caused by any increase in yield strength which accompanied an increase in hardness.

A similar, but less reliable correlation, also existed between hardness and fracture toughness in those composites which contained small (< 8 vol %), single additions of either TiC, NbC, or MnS; better correlation again existed between fracture toughness and matrix micro-hardness than with the bulk overall hardness of the composite.

Fracture toughness values in the M3/2 + TiC composites were almost identical to those found in the baseline M3/2 high-speed steel of equivalent matrix hardness, and were largely unaffected by the particulate addition. Crack propagation in this material was therefore unaffected by the presence of any small pre-existing cracks that were formed within TiC/MC clusters at stresses below the final fracture stress. Such behaviour must suggest that these individual cracked TiC/MC carbide clusters were too small, too isolated and too dispersed to influence crack propagation. The small number of cracked carbides that fell within a "damage process zone" [22, 23], at the crack tip was, therefore, below some required critical value. The size of this "damage process zone" would normally include any plastic zone at the crack tip where plastic deformation of the matrix could generate either ductile fracture or brittle cleavage through the matrix, plus an additional zone in which the local concentrated stress was high enough to cause cracking within or debonding around features such as the primary M_6C/MC carbides, TiC/MC and NbC clusters or MnS particles that lay ahead of the crack tip. Multiple cracking of primary carbide particles ahead of the main crack, and beyond the plastic zone, have been observed in high-speed steels [24], and in TiC particles present in Ferro-TiC® alloys [25], and also within some of these composites, see Fig. 10. "Damage process zones" were also seen in the composites that contained MnS because of debonding around MnS particles which took place so easily that the MnS particles could be regarded more or less as being mechanically equivalent to a void or pore [26]. Cracking of NbC clusters seen within the "damage process zone", could have taken place because of stresses generated at these carbides by the differences between the Young's modulus of the carbide and the steel. Load transfer between the matrix and the carbide should have occurred easily, because the NbC carbides were well bonded into the steel matrix, and any such carbide particles that were subjected to iso-strain conditions would experience higher localized stresses because of the fact that they have a higher Young's modulus than the surrounding high-speed matrix. Cracking of the TiC/MC clusters within the "damage process zone" might also have occurred for similar reasons, although these were less easily detected and did not show the same degree of crack branching as within the NbC clusters. The formation of larger macroscopic cracks by the coalescence of cracks formed in carbide clusters and by the debonding around particle boundaries, was eventually responsible for creating a critical-sized crack that generated catastrophic fracture.

Typical plastic zone sizes for the M3/2 baseline and the composites with single and double additions of TiC, NbC or MnS are shown in Table XIII and were calculated from the relationship: radius of plastic zone $R_p = 1/6\pi\,[K_{IC}/\sigma_{yld}]^2$, where K_{IC} is the fracture toughness, (MPa $m^{1/2}$), σ_{yld} the yield stress, which was estimated from the matrix micro hardness by the relationship that the stress required to cause tensile yielding is approximately one-third of that needed for hardness indentation, i.e. $\sigma_{yld} \approx (3.27\,H_m)$ MPa, and H_m is the micro-hardness of the steel matrix (kg mm^{-2}). Table XIII also includes the radius of a "damage process zone" in which micro-cracking or debonding around particles could occur and was calculated from average bend strength and the observations made for stresses required to nucleate cracks at the more important microstructural features of the various composites, see Tables IX and XII.

In the case of the TiC composite, the size of the "damage process zone" was small, so that cracking within any TiC/MC clusters could only occur within

TABLE XIII Calculated plastic zone sizes in heat-treated materials

Composite	Microhardness H_m ($kg\,mm^{-2}$)	Fracture toughness, K_{IC} ($MPa\,m^{1/2}$)	Radius of plastic zone, R_p (μm)	Identity and radius of "damage process zone", R_m (μm)
Baseline M3/2	624–982	32.8–17.4	1.5–13.7	M_6C; 7.4
M3/2 + 5% TiC	847	23.3	3.8	TiC/MC cluster; 9.3
M3/2 + 7.74% NbC	797	27.8	6.0	NbC cluster; 14.85
M3/2 + 5% MnS	714	24.6	5.9	de-bonded MnS; 32.7
M3/2 + 5% TiC + 5% MnS[a]	572–722	17.5–25.5	2.9–9.9	MnS/TiC cluster; 12.1
M3/2 + 7.74% NbC + 5% MnS	638–848	21.8–23.3	3.3–6.6	MnS/NbC interface; 38.8

[a]Low hardness did not necessarily indicate higher K_{IC} values, as little correlation existed between hardness and fracture toughness within the range of hardness and K_{IC} values quoted.

a few widely dispersed and isolated particles and for a short distance ahead of the crack tip; a mean spacing between TiC/MC clusters of approximately 40 μm was estimated by image analysis, and this was far larger than the size of the plastic zone. In this event crack propagation received little assistance from the presence of pre-cracked or de-bonded particles and was not affected by the small 8 vol % addition of TiC particles, because the large mean free path between TiC particles meant that the crack encountered so few of such particles along its complete crack front. Crack propagation was thus dependent almost totally on cracking within the steel matrix and was controlled by the fracture toughness particular to the heat-treatment state of the steel, as was found to be the case in other grades of high-speed steel [27].

Small changes in fracture toughness were, however, observed in the other two composites that contained single particulate additions, notably a slight decrease in K_{IC} due to the presence of 5% MnS, and a small increase in K_{IC} produced by the incorporation of 7.74% NbC. The small reduction in fracture toughness found with MnS additions was best explained by two main effects. Firstly, the 5 wt % addition of MnS used, corresponded to a somewhat higher volume fraction ($\approx$11 vol %), than was produced by using single additions of TiC or NbC carbide, and this relatively large volume fraction of MnS particles present meant that smaller bridging distances existed across any intervening matrix areas which made it easier for sub-critical growth to unite sub-cracks into the main crack. Lower fracture toughness values and hence easier crack propagation was also assisted by the fact that micro-cracking could occur so easily by debonding around MnS particles at relatively low stress and for some considerable distance ahead of the main crack tip. Further enhancement of crack propagation also included the possibility that cracks were attracted towards MnS particles by the residual stresses in the steel/MnS interface that were caused by differences between the thermal expansion characteristics of MnS and high-speed steel.

Thermal contraction on cooling is greater for MnS than for the high-speed steel matrix and would effectively cause either residual tensile stress to be set up in the surrounding steel matrix or debonding at the steel and MnS particle interface [16]. The large strain mismatch introduced by a large difference between the Young's moduli of MnS and high-speed steel could be responsible for relatively high tensile stresses being generated by this thermal contraction effect.

The effects of NbC carbides on fracture toughness were less easily explained and the small increase in fracture toughness found was contradictory to expectations in that the fracture toughness should have decreased in a manner consistent with the fact that the hardnesses of the heat-treated NbC composite were actually higher than in any other material. A reduction in the fracture toughness due to NbC carbide additions might also be anticipated because of the cracking of the NbC clusters ahead of the crack tip that was not only observed but also predicted by the relatively large "damage process zone" which extended well beyond the limits of the plastic zone, shown in Table XIII.

One possible explanation for the anomalous behaviour of the NbC composites lay in the fact that crack branching was extremely widespread within NbC clusters, see Fig. 10, although no particular microstructural feature, such as the boundary between NbC and M_6C carbides shown to exist inside the cluster, could be identified as the preferred path for such cracks. Branching of the microcracks formed in the NbC clusters ahead of the crack tip (damage process zone) thus appeared to cause stress relief and to act as a fracture energy dissipation mechanism [28, 29], which raised fracture toughness by restricting the ease of crack propagation. Micro-cracks formed alongside the propagating crack also remained as a "debris" layer on each side of the crack walls and could further dissipate energy from behind the advancing crack front. The toughening caused by this mechanism must, however, be relatively small for the same reasons argued previously, namely that only small volume fractions of NbC particles were present in this particular composite.

An additional explanation for the improved fracture toughness shown by the NbC composite over that of the baseline M3/2 high-speed steel of equivalent hardness, was that increases in the toughness of the high-speed steel matrix also occurred due to the effects of NbC on the secondary hardening produced by tempering. An ability to maintain hardness at higher tempering temperatures plus the more rapid secondary hardening response caused by the NbC carbide additions meant that it was possible to retain an equivalent matrix hardness to that found in the baseline M3/2, by using a higher tempering temperature.

The steel matrix of the NbC composite thus adopted a more toughened state due to the extra stress relief and the development of a more highly tempered condition within any tempered martensite present in the structure.

Composites which contained combined additions of ceramic carbide plus 5% or 15% MnS not only gave poor fracture toughness values but also showed that they possessed no correlation between fracture toughness and the hardness of the steel matrix. Changes in matrix hardness and bulk hardness due to different heat treatments had little influence on fracture toughness, and crack propagation was no longer determined by the properties or microstructure of the high-speed steel matrix but was instead controlled primarily by the quantity, size and distribution of the particulate-phase additions. The small interparticle spacing created by the presence of a high volume fraction of particles, together with the ease by which such particles could fracture within carbide/MnS clusters and by de-bonding around MnS clusters, easily promoted the growth and combination of microcracks into larger, critical sized cracks that were responsible for final catastrophic failure and low fracture toughness. This effect was particularly pronounced in the composites that contained high volume fractions (15 wt %, $\approx$ 30 vol %) of MnS combined with ceramic carbides, where very poor fracture toughness arose and was associated with crack propagation almost exclusively through a network of MnS/carbide clusters.

These findings support the suggestion that fracture toughness of metal matrix composites becomes dependent on the volume fraction, size, and distribution of added particles only at some critical level. Below this critical level, fracture toughness is governed by the microstructure and mechanical properties of the matrix; particles are either too small, too dispersed, or too few in number to influence fracture toughness, even though they may themselves crack at stresses below the final failure stress. Above the critical level, relatively large numbers of cracked particles, with a small mean free path between them, provides an easy path for crack propagation and a subsequent reduction in fracture toughness. Other authors [12, 30], agreed with these findings by demonstrating that the combined additions of TiC plus WC plus Mo_2C had an extremely deleterious effect on the fracture toughness of M2 high-speed steel, whereas single, low volume fraction additions, of TiC or VC carbides had little effect on the fracture toughness of an M3/2 high-speed steel [31].

4.1.3. Bend strength

The incorporation of either TiC or NbC ceramic carbides or MnS particles into the structure of M3/2 high-speed steel reduced bend strength in both the as-sintered and in the quenched and tempered material.

Bend strengths in composites which contained MnS particles were markedly lower than those of the baseline M3/2 high-speed steel. These reductions in strength were essentially caused by the effects of the particulate addition on the combined processes of crack initiation and crack propagation within the material, and the final bend strength of any of these materials ultimately depended on the size of any defects or micro-cracks present and the fracture toughness of the individual composite material.

Very poor bend strengths, shown by the reduced slopes at the lower strength end of the Weibull analysis plots, see, Fig. 1a–d, occurred when failure was initiated at defects that were already present, e.g. large pores inherited during sintering, that were of sufficient size to cause catastrophic fracture when the combination of applied bending stress and defect size reached a 'critical stress intensity, K_c' value.

Alternatively failure was initiated by cracks that were formed by the action of the applied bending stress, as was shown to occur by cleavage amongst the M_6C primary carbide population of the baseline M3/2 high-speed steel and by the debonding around MnS particles or by cleavage cracking within TiC/MC or NbC/M_6C clusters. Although these cracks might potentially be sufficiently large at birth to promote instantaneous/catastrophic crack propagation, it appeared more likely that they were initially sub-critical-sized cracks which progressively grew into larger cracks that eventually satisfied the critical size and "critical stress intensity, K_c" conditions needed for crack propagation.

In the mid to higher bend strength range covered by the Weibull analysis, less uncertainty in fracture behaviour occurred and fairly high Weibull moduli were achieved; probably because fracture in this range was less likely to be associated with pores and was more likely to have been initiated by the micro-cracking of primary carbides or of particle clusters introduced by the additions of ceramic carbides and MnS particles.

Lower Weibull moduli, and therefore greater uncertainty in fracture behaviour, occurred within the composites than in the baseline material M3/2 high-speed steel, possibly because the composites contained a greater variation in size and a less homogeneous distribution of potential fracture initiation sites; composites which included MnS particles were again worst in this respect. Smaller variations in the size and shape of the NbC/M_6C clusters combined with the higher K_{IC} fracture toughness of the NbC composite tended to give this composite a higher Weibull modulus and intrinsically higher bend strength than the TiC counterparts. Considerable variations in the size of TiC/MC clusters occurred, and occasionally extremely large TiC/MC clusters were observed in the M3/2 plus TiC composite.

Experimental evidence, see Table XII, clearly showed that sub-critical cracks associated with cleavage in carbide clusters or debonding around MnS particles were formed at stresses well below the final bend strength and that some form of sub-critical crack growth must have occurred prior to final failure. Some caution must be exercised, however, before assigning blame for the damage caused to the bend strength to all of the cracks observed on the polished tensile face of the bend test specimens. Many of the cracks seen on

the pre-polished tensile face have been shown by previous authors [32], to consist of exceedingly shallow surface cracks which were largely non-propagating and did not penetrate far below the specimen surface. Development into a critical-sized defect required growth of any microcracks into a semi-circular flaw that was dependent on the local microstructure being conducive to the formation of semi-circular microcracks: such effects as any lack of inherent ductility within the surrounding matrix, or a small separation between isolated cracks in brittle particles, would assist the linking together of small cracks to form a larger critical-sized crack.

Some attempt to evaluate critical defect sizes that could explain the observed bend strength values was made by applying the flaw-shape parameter, Q, used to describe either semi-elliptical surface or buried elliptical flaws of different $a/2c$ aspect ratios [6]. Q varies as a function of crack length, $2c$, depth a, and the ratio σ/σ_y; where σ is the applied stress, and σ_y the yield stress (estimated from matrix micro-hardness).

For a semi-elliptical surface flaw, the critical flaw parameter $(a/Q)_{cr} = 1/1.21\pi(K_{IC}/\sigma)^2$, and for an elliptical embedded flaw, $(a/Q)_{cr} = 1/\pi(K_{IC}/\sigma)^2$

Typical surface flaw sizes, calculated via these relationships for the range of crack aspect ratios 0.1–0.5, and at σ/σ_y ratios appropriate to the measured bend strength and at a yield stress estimated from matrix micro-hardness of the individual composite, are shown in Table XIV. The lower values of a_{cr} and $2c_{cr}$ shown by this table corresponded to a semi-circular surface crack and were probably a more accurate estimate of critical crack sizes required to cause bending failure [32].

The measured size of individual features such as the primary matrix M_6C carbides, individual TiC or NbC ceramic carbide particles, TiC/MC or NbC/MC carbide clusters, MnS and or MnS/carbide clusters that were known to be capable of nucleating micro-cracks, were all somewhat smaller than the critical crack sizes shown by Table XIV.

More precise measurements of critical defect size and the exact relationship between bend strengths, and K_{IC} fracture toughness of the individual materials could not be assessed, simply because the actual K_c (critical stress intensity) value responsible for final catastrophic fracture probably differed from the measured value of K_{IC} for a number of reasons. Critical stress intensity levels required for crack propagation with short cracks at the micro level, are known to be less than K_{IC} which refers to the propagation of large macroscopic cracks [33]. Additional problems in estimating K_c also arise from possible variations in flaw shape parameter that could occur with different types of crack-initiating site, changes in local crack opening mode, and the possible absence of plane strain conditions at the defect responsible for initiating bend stress failure.

Despite this problem, however, it appeared most likely that the bend strengths of the composites were usually controlled by the ease by which sub-critical cracks could first grow to some critical size and then by the fracture toughness of the matrix which determined the point at which this crack became capable of causing catastrophic fracture. The low stresses needed to initiate and grow micro-cracks in composites that contained MnS additions, combined with an inherently poor fracture toughness, meant that these materials gave rise to the lowest bend strength, particularly when cracks could easily travel through an almost continuous network of MnS/carbide clusters such as produced in those composites with 15 wt % MnS present.

5. Conclusions

1. The addition of 5% TiC or 7.74% NbC to M3 class 2 high-speed steel slightly increased the overall (i.e. macro-) hardness relative to the M3/2 baseline material. Slight softening of the steel matrix occurred with the TiC-based composite due to the conversion of the M_6C carbides into MC carbides within the steel matrix. The highest hardness values achieved by heat treatment occurred in the M3/2 + NbC composites and this was attributed to slight dissolution of NbC into the high-speed steel matrix which gave an improvement in secondary hardening after tempering. MnS additions caused a marked drop in bulk hardness but had little effect on the hardness of the M3/2 steel matrix.

TABLE XIV Critical crack sizes calculated as being required to cause fracture at the observed bend strength of heat-treated composites

Material	σ (MPa)	K_{IC} (MPa m$^{1/2}$)	Estimated σ_{yld} (MPa)	σ/σ_{yld}	Q range	Depth a_{cr} (μm)	Length $2c_{cr}$ (μm)
Baseline M3/2	2677	19.9	2592	1.00	0.88–2.4	13–35	128–69
5% MnS	1829	23.3	2541	0.72	0.97–2.25	41–96	414–192
5% TiC	1711	24.6	2142	0.80	0.95–2.30	52–125	517–250
7.74% NbC	1910	27.8	2391	0.80	0.95–2.30	53–128	529–256
5% MnS + 5% TiC	1262	25.7	2025	0.62	1.01–2.22	110–242	1110–484
5% MnS + 7.74% NbC	1141	22.9	2364	0.48	0.93–2.18	99–231	985–462
15% MnS + 5% TiC	720	13.2	2142	0.34	0.83–2.16	73–191	730–382
15% MnS + 7.74% NbC	747	14.0	2205	0.34	0.83–2.16	77–200	770–400

2. All three particulate additions had a deleterious effect on three-point bend strength, particularly in the case of MnS addition. Bend strengths were further reduced by the simultaneous addition of both MnS and either TiC or NbC, especially when a high volume fraction of approximately 25 vol % MnS was added.

3. Single, low volume fraction ($\leqslant 8\%$) additions, of TiC, NbC, or MnS, had little effect on fracture toughness and K_{IC} values were comparable to those found in the baseline M3/2 steel. Slight improvements in fracture toughness shown to occur in the 7.74% NbC composites were attributed to energy dissipation caused by the effects of crack branching during crack propagation and to improvements in the toughness of the tempered martensite formed during tempering. Composites with the higher volume fraction additions of MnS and ceramic carbide gave poor fracture toughness by forming MnS/carbide clusters which provided an easy path for crack propagation.

4. Fracture initiation was found to occur via the formation of micro-cracks within various structural features of the microstructure. Primary M_6C and MC carbides, with a slight preference for cleavage across M_6C carbides, provided a source of fracture initiation in the M3/2 baseline steel. Crack initiation was seen in clusters of TiC/MC or NbC/M_6C carbide agglomerates formed during sintering and also occurred very easily by debonding at the MnS/steel matrix interface.

5. Cracked carbide agglomerates or de-bonded MnS particles formed by the application of stress, were initially not large enough to cause catastrophic fracture. Growth of these subcritical flaws into a critical-sized defect prior to final catastrophic fracture was thought to occur.

6. The introduction of ceramic carbides and MnS particles into the high-speed steel caused some reduction in reliability with regards to their failure stress. A Weibull modulus of approximately 15 was achieved for the three-point bend strength of the baseline M3/2 steel but this was reduced to values of between 8 and 11 by the introduction of particulate additions. Bimodal slopes found for some of the Weibull analysis indicated that different defect types could be responsible for failure initiation and that the poorest bend strength values occasionally observed were probably initiated by pores.

Acknowledgements

The authors acknowledge the invaluable help and co-operation of all of the partners involved in the BRITE/EURAM project which formed the basis of this work. These include; AMES, Spain; Hoganas, Sweden; Iveco, Italy; SMK Krebsoge, Germany; and Sintertech, France. Thanks are also due to Professor A. S. Wronski, University of Bradford, for his help in interpreting the fracture toughness results.

References

1. E. VANNMAN, Hoganas AB, Sweden, BRITE/EURAM Project, BREU 0439, Project no. 4028 (1995).
2. J. D. BOLTON and A. J. GANT, *Powder Metall.* **36** (1993) 267.
3. British Standard B S 5447: Plane strain fracture toughness of metallic materials (BSI London, 1997).
4. K. ERIKSSON, *Scand. J. Metall.* **2** (1973) 197.
5. J. E. KNOTT, "Fundamentals of Fracture Mechanics" (Butterworths, London, 1976).
6. J. F. KNOTT and D. ELLIOT, "Worked Examples in Fracture Mechanics", Monograph no.4 (Institution of Metallurgists, London, 1979).
7. E. PAPADAKIS, in "Physical Acoustics Principles and Methods" vol. 12, edited by W.P. Mason and R.N. Thurson, (Academic Press, New York, 1976) 1285.
8. J. D. BOLTON and A. J. GANT, *Powder Metall.* **39** (1) (1996) 27.
9. W. WEIBULL, *J. Mech. Phys. Solids* **8** (1960) 100.
10. C. CHATFIELD, "Statistics for Technology", 3rd Edn (Chapman and Hall, London, 1983).
11. P. BEISS, R. WAHLING and D. DUDA, "Modern Developments in Powder Metallurgy", Vol. 17 (MPIF, Princeton, NJ, 1985) p. 331.
12. P. W. SHELTON and A.S. WRONSKI, *Metal Sci.* **17** (1983) 533.
13. M. M. OLIVEIRA, J. MASCARENHAS and A. S. WRONSKI, *Powder Metall.* **36** (1993) 281.
14. M. SANTOS, M. M. OLIVEIRA, M. M. REBBECK and A. S. WRONSKI, *ibid.* **34** (1991) 93.
15. G. HOYLE, "High Speed Steel", (Butterworths, London, 1988).
16. D. BROOKSBANK and K. W. ANDREWS, *JISI* **210** (1972) 246.
17. R. W. HERTZBERG, "Deformation and Fracture Mechanics of Engineering Materials", 3rd Edn. (Wiley, New York, 1989), 14.
18. R. H. KROCK, *ASTM Proc.* **63** (1963).
19. A. J. GANT, PhD thesis, University of Bradford (1996).
20. J. D. BOLTON, M. JEANDIN and C. JOUANNY TRESY, *Powder Metall.* **33** (1990) 126.
21. G. BERRY and M. J. K. Al-TORNACHI, *Metal. Technol.* **6** (1977) 289.
22. W. D. KINGERY, H. K. BOWEN and D. R. UHLMANN, "Introduction to Ceramics", 2nd Edn (Wiley, London, (1970).
23. F. L. MATHEWS and R. D. RAWLINGS, "Composite Materials, Engineering and Science" (Chapman and Hall, London, 1994).
24. A. IQBAL and J. E. KING, *Int. J. Fatigue* **12** (4) (1990) 234.
25. T. S. SRIVASTSAN, A. RAVINDRA, J. M. PANCHAL and A. PRAKASH, *Compos. Engng* **3** (1993) 329.
26. Y. MURAKAMI and M. ENDO, *Fatigue* **16** (4) (1994) 163.
27. M. A. GOMES, A. S. WRONSKI and C. S. WRIGHT, *Fatigue Fract. Engng Mater. Struct.* **18** (1) (1995) 1.
28. R. STEINBRECH, R. KHEHANS and W. SCHWAARWACHTER, *J. Mater. Sci.* **18** (1983) 265.
29. A. G. EVANS and K. T. FABER, *J. Amer. Ceram. Soc.* **67** (1984) 255.
30. P. W. SHELTON, M Phil thesis, University of Bradford (1979).
31. J.D. BOLTON and M. YOUSEFFI, *Powder Metal.* **36** (2) (1993) 142.
32. M. A. R. GOMES, PhD thesis, University of Bradford, (1993).
33. K. J. MILLER, *Mater. Sci. Technol.* **9** (1993) 453.

Received 3 February
and accepted 24 September 1997